Scientific Bulletin of the
Politehnica University of Timisoara
Transactions on Mechanics Special issue

The 6th International Conference on
Hydraulic Machinery and Hydrodynamics
Timisoara, Romania, October 21 - 22, 2004

SWIRLING FLOW DOWNSTREAM A FRANCIS TURBINE RUNNER

Romeo SUSAN-RESIGA, Professor*
Department of Hydraulic Machinery
"Politehnica" University of Timişoara

Gabriel Dan CIOCAN, PhD.
Laboratory for Hydraulic Machines
École Polytechnique Fédérale de Lausanne

François AVELLAN, Professor
Laboratory for Hydraulic Machines
École Polytechnique Fédérale de Lausanne

**Corresponding author*: Bvd. Mihai Viteazu 1, RO-300222, Timisoara, Romania
Tel.: (+40) 256 403692, Fax: (+40) 256 403700, Email: resiga@mh.mec.utt.ro

ABSTRACT

An analytical representation for swirling flow at the Francis runner outlet is built using a superposition of three elementary vortices. The first vortex corresponds to a rigid body rotation, with a constant axial velocity profile. The other two vortices are of Batchelor type: one is counter-rotating and co-flowing, while the other is co-rotating and counter-flowing with respect to the first vortex. The mathematical analysis of this vortex system shows that the swirl reaches a critical state practically at the same discharge value where a sudden variation in the draft tube pressure recovery is experimentally observed. We recommend that when designing a Francis turbine runner one should avoid reaching a critical state for the swirl at the runner outlet within the normal operating range.

KEYWORDS

Francis turbine, swirling flow

NOMENCLATURE

V_a dimensionless axial component of velocity
V_u dimensionless circumferential component of velocity
R_s dimensionless radius of survey section
R_1, R_2 dimensionless vortex core radii
Ω_0, Ω_1, Ω_2 dimensionless angular velocities
U_0, U_1, U_2 dimensionless axial velocities
r dimensionless radius
φ discharge coefficient
ψ streamfunction
κ axi-symmetric perturbation wavenumber

1. INTRODUCTION

Swirling flow behavior in various technical applications has long been an intensive subject of research. Usually swirl effects are seen as either the desired result of design or unavoidable, possibly unforeseen, side effects. However, the hydraulic turbine draft tube on one hand benefits from the swirl at runner outlet in order to mitigate flow detachment in the cone, but on the other hand suffers from flow instabilities leading to draft tube surge.

The draft tube of a hydraulic turbine is the machine component where the flow exiting the runner is decelerated, thereby converting the excess of kinetic energy into static pressure. In the case of machine rehabilitation of an existing power plant mostly only the runner and the guide vanes are currently modified. For economical and safety reasons, the spiral casing and the draft tube are seldom redesigned, even if these components present some undesirable behavior. When re-designing the runner, the swirling flow structure at the draft tube inlet generally changes with respect to the original design, and as a result the flow in the turbine draft tube may be significantly different at the same discharge, even if the draft tube geometry remains the same. As a result, it is important to evaluate the characteristics of the swirling flow ingested by the draft tube, in order to avoid peculiar and undesirable sudden variations in the draft tube pressure recovery coefficient when varying the discharge.

The obvious practical importance of predicting the complex flow downstream the turbine runner, in the draft tube, led to the FLINDT research project of Flow Investigations in Draft Tubes [1]. The main objective of this project was to investigate the flow in hydraulic turbines draft tubes, for a better understanding of the physics of these flows and to build up an extensive

experimental data base describing a wide range of operating points which can provide a firm basis for the assessment of the CFD engineering practice in this component. The extensive experimental investigation of the draft tube flow has been complemented with three-dimensional numerical flow simulations [5,6] aimed at elucidating the swirling flow evolution up to the turbine outlet as well as the phenomena that led to the peculiar sudden drop in turbine efficiency.

The present paper focuses on the structure of the swirl produced by the constant pitch turbine runner and further ingested by the draft tube. The corresponding hydrodynamic field is a direct outcome of the runner design and the operating point. Since changing the runner design, while keeping the same draft tube, may lead to unexpected sudden efficiency drop for a certain discharge it would be preferable that some design criteria be put forward as far as the runner outlet swirl is concerned. The present analysis shapes such criteria by using relative simple mathematical and numerical tools. If the runner outlet swirl structure displays a sudden change with respect to appropriate criteria, and this change occurs at a discharge close to the experimental one where the sudden drop in turbine efficiency is observed, these criteria should be taken into account when designing or re-designing the runner.

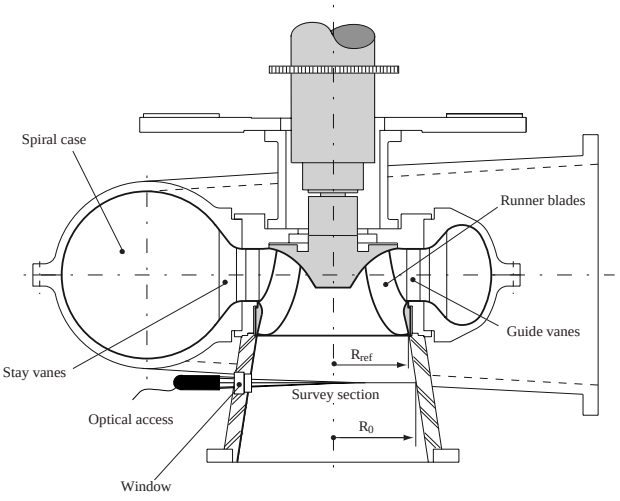

Figure 1. Sketch of the Francis turbine model and the LDA setup for the flow survey section at runner outlet.

The FLINDT project experimental investigations were carried out on a Francis turbine scaled model of specific speed 0.56, Fig. 1. The experimental data used in this paper were obtained with a two components probe Laser Doppler Anemometer, using back-scattered light and transmission by optical fiber, with a LASER of 5W Argon-ion source. The measuring point geometrical location is controlled within a 0.05 mm accuracy. Both axial and circumferential components of the velocity were measured on the survey section from Fig. 1. The uncertainties of the velocity measurements are estimated to be 2% of the measured value. Throughout this paper the velocity is made dimensionless by the *runner angular speed* $\times$ *runner outlet radius*, and lengths are made dimensionless with respect to the *runner outlet radius*, R_{ref} in Fig. 1.

2. ANALYTICAL REPRESENTATION OF AXIAL AND CIRCUMFERENTIAL VELOCITY PROFILES

Several swirling flow models have been considered in the literature to study either the vortex stability or the vortex breakdown. A rigorous theoretical foundation is provided for the Burgers' vortex (also known as Lamb vortex) which gives the circumferential velocity profile (1a).

$$V_u(r) = \Omega \frac{R^2}{r}\left[1-\exp\left(-\frac{r^2}{R^2}\right)\right], \qquad (1a)$$

$$V_u(r) = \begin{cases} \dfrac{\Omega R^2}{r} & \text{for } r \geq R, \\ \Omega r & \text{for } r \leq R. \end{cases} \qquad (1b)$$

In Eq. (1a) Ω denotes the angular velocity in the vortex axis, and R is the vortex core radius. This physical interpretation is obvious for the Rankine vortex (1b), which considers the asymptotic behaviour of the Burgers vortex for large and small radius values.

It was Batchelor [2] who pointed out that a radial variation in circumferential velocity must be accompanied by a variation in the axial velocity. Faller and Leibovich [4] have used the following axial velocity functional form to fit their experimental data for a radial guidevanes swirl generator,

$$V_a(r) = U_0 + U_1 \exp\left(-\frac{r^2}{R^2}\right), \qquad (2)$$

where U_1 is the difference between the axial velocity on the axis and the axial velocity far away from the axis, U_0. Note that when using (2) together with (1a) the vortex core radius R is the same.

Based on the analysis of the experimental data for the swirling flow downstream a Francis turbine runner we have concluded, [7], that both circumferential and axial velocity profiles can be accurately represented using a superposition of elementary vortices:

$$V_u(r) = \Omega_0 r + \Omega_1 \frac{R_1^2}{r}\left[1-\exp\left(-\frac{r^2}{R_1^2}\right)\right] + \Omega_2 \frac{R_2^2}{r}\left[1-\exp\left(-\frac{r^2}{R_2^2}\right)\right], \qquad (3)$$

$$V_a(r) = U_0 + U_1 \exp\left(-\frac{r^2}{R_1^2}\right) + U_2 \exp\left(-\frac{r^2}{R_2^2}\right). \qquad (4)$$

If R_s is the dimensionless survey radius, then the discharge coefficient can be obtained by integrating the axial velocity profile (4),

$$\varphi = U_0 R_s^2 + U_1 R_1^2 \left[1 - \exp\left(-\frac{R_s^2}{R_1^2}\right)\right] \qquad (5)$$
$$+ U_2 R_2^2 \left[1 - \exp\left(-\frac{R_s^2}{R_2^2}\right)\right].$$

The functional forms (3) and (4) have an eight parameter set $\mathbf{\Pi} \equiv \{R_1, R_2, \Omega_0, \Omega_1, \Omega_2, U_0, U_1, U_2\}$ to be determined by fitting the experimental data. For each turbine operating point under consideration, with a set of experimental data $(r, V_a, V_u)_j$, $j = 1, \ldots, N$, the error vector $\mathbf{e}(\mathbf{\Pi}) = \{e_k(\mathbf{\Pi})\}, k = 1, 2, \ldots, 2N$ is defined as

$$e_k(\mathbf{\Pi}) = \begin{cases} V_a(r_k, \mathbf{\Pi}) - (V_a)_k, & k = 1, 2, \ldots, N, \\ V_u(r_{k-N}, \mathbf{\Pi}) - (V_u)_{k-N}, & k = N+1, \ldots 2N. \end{cases} \qquad (6)$$

The error vector includes both axial and circumferential velocity data since the vortex core radii R_1 and R_2 correspond to both velocity components. The parameter set is found by minimizing $\sum_{k=1}^{2N} [e_k(\mathbf{\Pi})]^2$, leading to a least-squares estimate of $\mathbf{\Pi}$. Let $\mathbf{\Pi}_c$ be the current estimate of $\mathbf{\Pi}$. A new estimate is given by $\mathbf{\Pi}_c + \mathbf{\Pi}_c^*$, where $\mathbf{\Pi}_c^*$ is a solution to

$$[\mathbf{J}^T(\mathbf{\Pi}_c)\mathbf{J}(\mathbf{\Pi}_c) + \mu_c \mathbf{I}]\mathbf{\Pi}_c^* = \mathbf{J}^T(\mathbf{\Pi}_c)\mathbf{e}(\mathbf{\Pi}_c) \qquad (7)$$

Here $\mathbf{J}(\mathbf{\Pi}_c)$ is the Jacobian $(2N) \times 8$ matrix evaluated analytically at $\mathbf{\Pi}_c$. The iterative algorithm uses a "trust region" approach with a step bound of δ_c. A solution of Eqs. (5) is first obtained for $\mu_c = 0$. If $\|\mathbf{\Pi}_c^*\|^2 < \delta_c$ this update is accepted. Otherwise, μ_c is set to a positive value and another solution is obtained.

Circumferential and axial velocity profiles on the survey section are fitted with Eqs. (3) and (4) for 17 operating points. Table 1 shows the measured discharge coefficient as well as the value computed with Eq. (5) and the error with respect to the measured value. This error is a good indicator for the accuracy of the fit, as well as for the measurements overall accuracy. Moreover, we can conclude that Eq. (4) is a very good representation for the axial velocity profile at the runner outlet. As far as the circumferential velocity is concerned, the superposition of three vortices in Eq. (3) accurately represents the experimental data over the whole discharge range under investigation.

Figures 2-7 display the data as well as the curves fitted for the first six operating points from Table 1. These operating points cover the investigated discharge domain at a constant head corresponding to the turbine best efficiency operating point. The quality of the fit can be assessed by observing that most of the time the curves approach the experimental points within the measurement errors of 2%. The wall boundary layer is not correctly reproduced since the swirling flow model (3,4) was specifically built for an inviscid flow analysis.

A main goal of this investigation is to find a suitable parametric representation for the swirling flow at the Francis runner outlet. Figure 8 shows the variation of the vortex characteristic angular velocities with respect to φ. Linear least squares fits accurately represent $\Omega_0(\varphi)$ and $\Omega_1(\varphi)$, while for $\Omega_2(\varphi)$ a parabolic fit seems to be quite satisfactory. Moreover, one should note that $\Omega_0(\varphi)$ is almost constant over the investigated operating range. The variation of vortex characteristic velocities with respect to φ is shown in Fig. 9, together with the corresponding linear fits. Finally, Fig. 10 displays the dependence of the vortex core radii on φ. A first conclusion from Figures 8-10 is that the swirl parameters in (3,4) have a smooth, generally linear, variation in φ over the investigated range.

Table 1. Measured and computed discharge coefficient for 17 operating points

Exp. φ	Energy Coeff.	Speed [rpm]	Comput. φ	Error [%]
0.340	1.18	1000	0.344	+1.1
0.360	1.18	1000	0.363	+0.8
0.368	1.18	1000	0.372	+1.0
0.380	1.18	1000	0.381	+0.2
0.390	1.18	1000	0.389	-0.2
0.410	1.18	1000	0.409	-0.3
0.368	1.00	1000	0.368	+0.1
0.380	1.00	1000	0.380	+0.1
0.370	1.11	1000	0.369	-0.1
0.368	1.30	1000	0.371	+0.8
0.380	1.30	1000	0.386	+1.5
0.410	1.30	1000	0.407	-0.6
0.370	1.11	500	0.370	+0.1
0.340	1.18	500	0.345	+1.6
0.368	1.18	500	0.369	+0.2
0.380	1.18	500	0.379	-0.3
0.410	1.18	500	0.406	-0.9

A qualitative picture of the three vortex system emerges from the above analysis. Vortex 0 is a rigid body rotation with angular speed Ω_0 and we can associate with it a

constant axial velocity U_0. *Vortex 1*, which has a vortex core extent about half the wall radius, is counter-rotating and co-flowing with respect to *Vortex 0*. The strength of this vortex, both in Ω_1 and in U_1, is growing as the flow-rate increases. *Vortex 2* has a core at least four times smaller than *Vortex 1*, is co-rotating and counter-flowing with respect to *Vortex 0*, and its strength increases as the flow-rate decreases. Note that as the flow-rate increases (eventually beyond the upper limit in our investigation) *Vortex 2* will vanish. These two

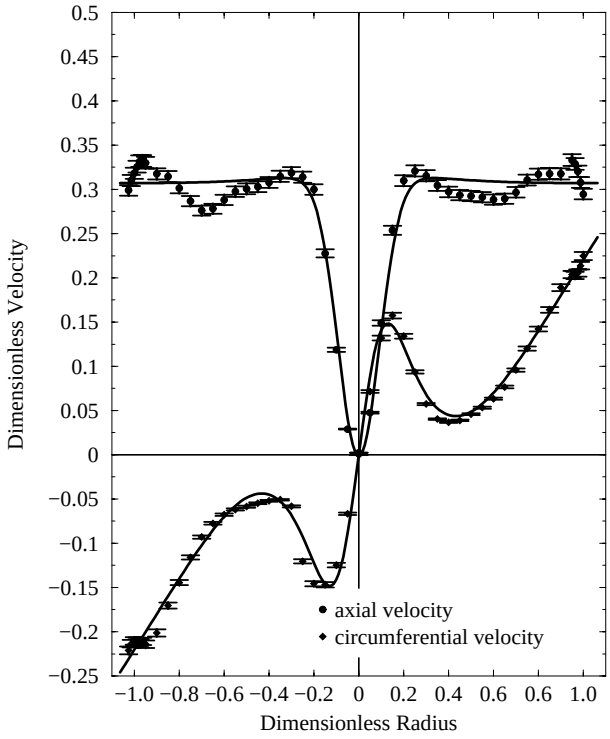

Figure 2. Axial and circumferential velocity profiles at discharge $\varphi = 0.340$.

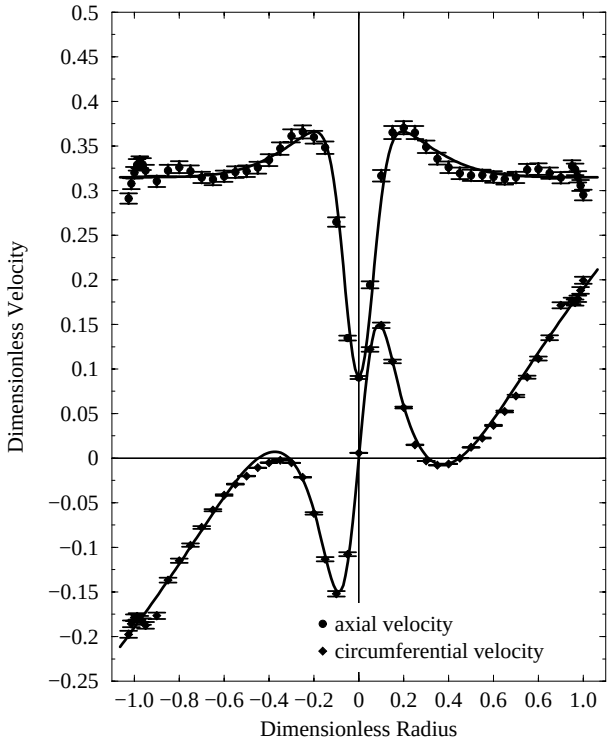

Figure 3. Axial and circumferential velocity profiles at discharge $\varphi = 0.360$.

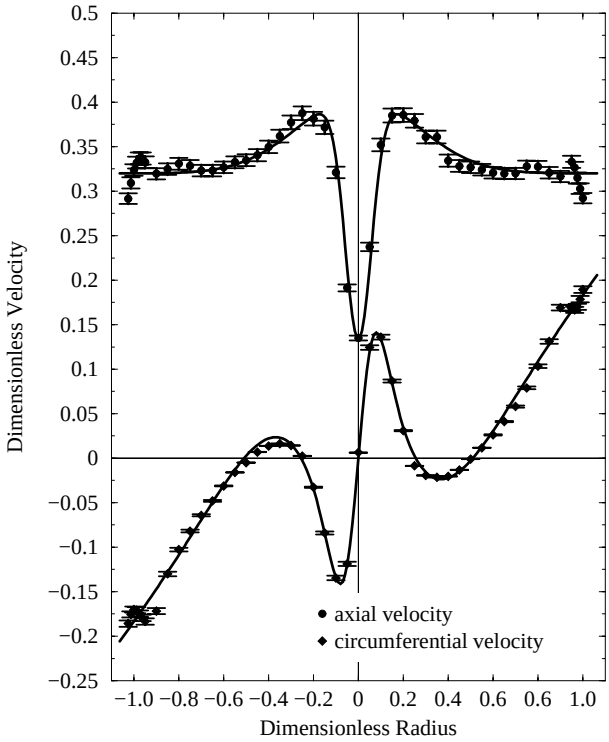

Figure 4. Axial and circumferential velocity profiles at discharge $\varphi = 0.368$.

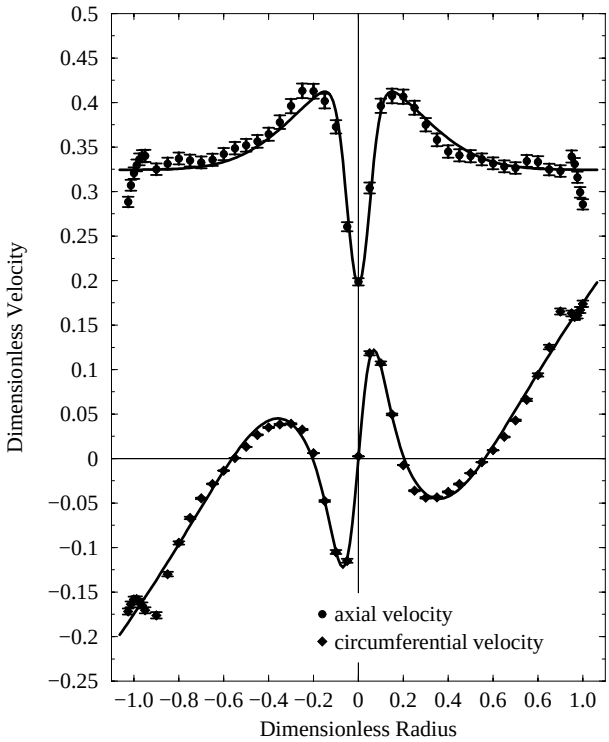

Figure 5. Axial and circumferential velocity profiles at discharge $\varphi = 0.380$.

Batchelor vortices are mainly responsible for the swirling flow behaviour. For φ smaller than the design value a wake-like axial velocity is developed, Fig. 2, while for larger φ the axial velocity has a jet-like profile, Fig. 7.

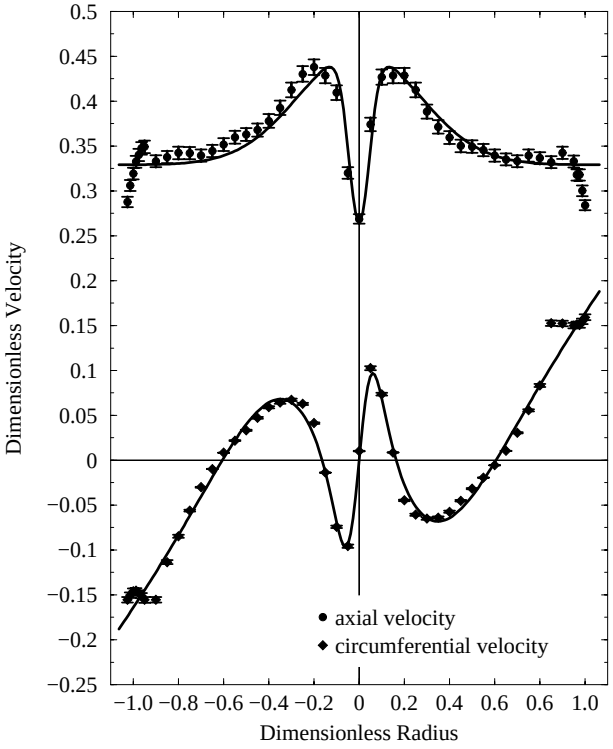

Figure 6. Axial and circumferential velocity profiles at discharge $\varphi = 0.390$.

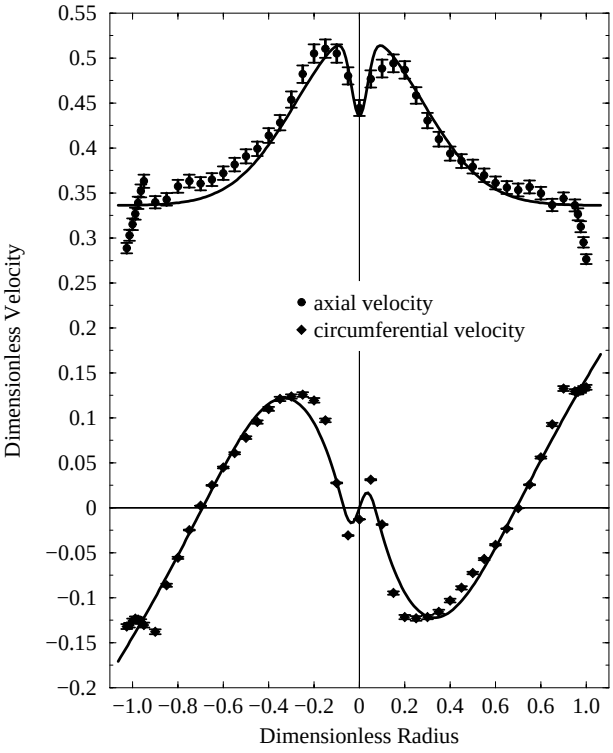

Figure 7. Axial and circumferential velocity profiles at discharge $\varphi = 0.410$.

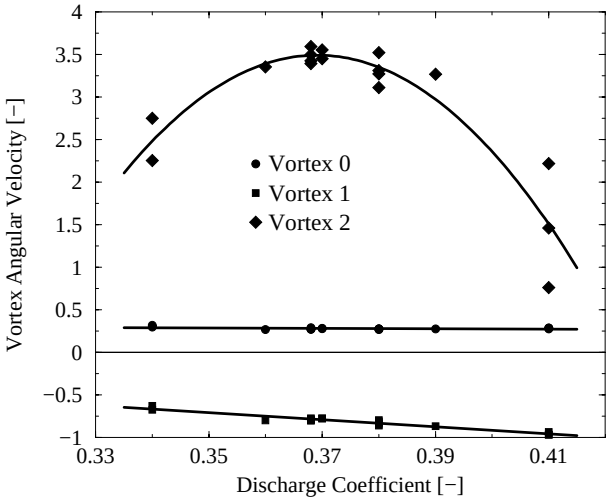

Figure 8. Characteristic angular velocities Ω_0, Ω_1, and Ω_2 versus discharge coefficient φ.

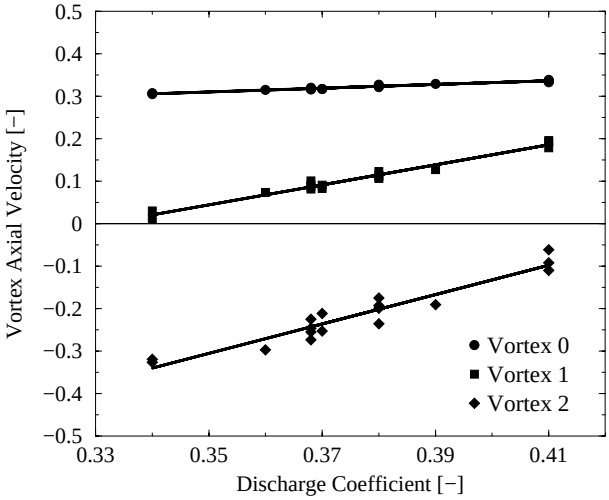

Figure 9. Characteristic axial velocities U_0, U_1, and U_2 versus discharge coefficient φ.

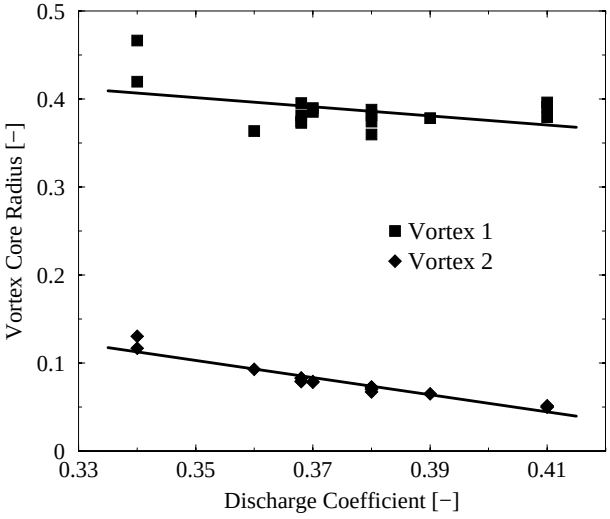

Figure 10. Vortex core radii R_1 and R_2 versus discharge coefficient φ.

3. ANALYSIS OF THE SWIRLING FLOW

Theoretical analysis of swirling flows can employ tools ranging from simplified axisymmetric, inviscid steady or unsteady flow models to full 3D laminar or turbulent numerical simulation. However, it is useful to first examine the swirling flow at the draft tube inlet before performing an analysis of the flow in the straight cone even in the whole 3D geometry. Such results may be quite useful if there is a correlation (even qualitative) with the overall draft tube behavior.

We consider a steady mean flow with axial and circumferential velocity profiles derived from experimental data in previous section. An inviscid incompressible fluid is considered, since our swirling flow representation does not account for the boundary layer near the wall. The radial velocity is negligible (generally one order of magnitude smaller) with respect to the axial velocity. Within these assumptions, the mathematical model further considered corresponds to the theory of finite transitions between frictionless cylindrical flows, originally developed by Benjamin [3]. The equation of continuity for axisymmetric incompressible flows is automatically satisfied by introducing the streamfunction $\psi(z,r)$ such that the axial and radial velocity components can be written as

$$V_a = \frac{1}{r}\frac{\partial \psi}{\partial r} \text{ and } V_r = -\frac{1}{r}\frac{\partial \psi}{\partial z} \tag{8}$$

From the axial velocity profile (3), the streamfunction can be readily written

$$\psi(r) = U_0\frac{r^2}{2} + U_1\frac{R_1^2}{2}\left[1-\exp\left(-\frac{r^2}{R_1^2}\right)\right] + U_2\frac{R_2^2}{2}\left[1-\exp\left(-\frac{r^2}{R_2^2}\right)\right] \tag{9}$$

When applied to a circuit around a particular streamsurface $\psi = \text{constant}$ Kelvin's theorem shows rV_u to be a constant. Thus in general $rV_u \equiv K(\psi)$, where K is a function of ψ alone. Also, on a streamsurface the total specific energy $H = p/\rho + \left(V_a^2 + V_u^2 + V_r^2\right)/2$ is constant by Bernoulli's theorem, thus H is a function of ψ alone. The momentum equation for the steady, axisymmetric swirling flow becomes

$$\frac{1}{r^2}\left(\frac{\partial^2\psi}{\partial z^2} + \frac{\partial^2\psi}{\partial r^2} - \frac{1}{r}\frac{\partial\psi}{\partial r}\right) = H'(\psi) - \frac{K(\psi)K'(\psi)}{r^2} \tag{10}$$

which is known in literature as Long-Squire or Bragg-Hawthorne equation. The prime denotes differentiation with respect to ψ. The solution of the non-linear Eq. (10) may be non-unique. To investigate this feature, the streamfunction is written as

$$\psi(z,r) = \Psi(r) + \varepsilon\tilde{\psi}(r)\exp(\mathrm{i}\kappa z), \tag{11}$$

where $\Psi(r)$ is the base flow given by Eq. (9), $\tilde{\psi}$ is a perturbation of the base flow, and κ is the axial wavenumber of this perturbation.

Substituting (11) in (10) one obtains a linear equation for $\tilde{\psi}$ with homogeneous boundary conditions (since $\tilde{\psi}$ does not change the overall flow rate). This eigenvalue problem allows the determination of the eigenvalues κ^2 and the corresponding eigenvectors. The Finite Element discretization procedure and numerical method are detailed in [7].

If $\kappa^2 < 0$ then κ is imaginary and the exponential factor in (11) will be $\exp(\pm|\kappa|z)$. As we move downstream the survey section, $z > 0$, the only physically acceptable solution corresponds to $\exp(-|\kappa|z)$, showing an exponential damping of $\tilde{\psi}$. A swirl configuration for which all eigenvalues are negative is unable to sustain axisymmetric small-disturbance standing waves and it was termed *supercritical* by Benjamin [3]. On the other hand, if at least one eigenvalue κ^2 is positive, then the perturbation will take the form of a standing wave $\exp(\pm\mathrm{i}\kappa z)$, and the corresponding flow is termed *subcritical*.

In this paper we examine the transition of the swirling flow downstream a Francis turbine runner from subcritical to supercritical as the discharge coefficient increases, and correlate the critical state with the experimentally observed sudden drop in the draft tube pressure recovery coefficient, Fig. 11.

For $\varphi > 0.365$ all eigenvalues are negative, thus the flow is supercritical and cannot sustain axisymmetric standing waves. However, for $\varphi < 0.365$ the largest eigenvalue becomes positive, followed by the next eigenvalue as φ decreases, and the flow is subcritical with standing waves described by the corresponding eigenvectors $\tilde{\psi}$. The critical state occurs, according to our computations, at $\varphi = 0.365$. This discharge value is quite close (only 1.3% smaller) to the value of $\varphi = 0.37$ where the sudden drop in the draft tube pressure recovery is observed.

It seems reasonable to assume that the critical state is directly related to this experimentally observed phenomenon, since by trying several draft tube geometries while keeping the same runner (and the swirling flow) the same behavior has been observed practically at the same discharge. While reaching the critical

swirl configuration seems to be the cause, the actual physical mechanism by which the pressure recovery suffers an abrupt change cannot be inferred from the present analysis. Experimental [1] as well as numerical [5,6] investigations offer a comprehensive analysis of the Francis turbine draft tube flow.

4. CONCLUSIONS

The present work started from the idea that the swirling flow configuration at the outlet of a Francis turbine runner has a major influence on the overall behaviour of the flow downstream in the draft tube. We have developed an analytical representation for the axial and circumferential velocity components at the outlet of a Francis runner, and the least-squares procedure to compute the model parameters. It is shown that the swirling flow in the survey section can be accurately represented using a superposition of three distinct vortices: a rigid body rotation motion, a counter-rotating and co-flowing Batchelor vortex with large core radius, and a co-rotating and counter-flowing Batchelor vortex with small vortex core.

The eight parameters of this model are shown to vary smoothly (generally linear) with the discharge coefficient. The flow at the runner outlet is analyzed using the mathematical model for a steady, axisymmetric and inviscid swirling flow. Following Benjamin's theory of finite transitions between frictionless cylindrical flows we have performed an eigenvalue analysis of the linearized problem.

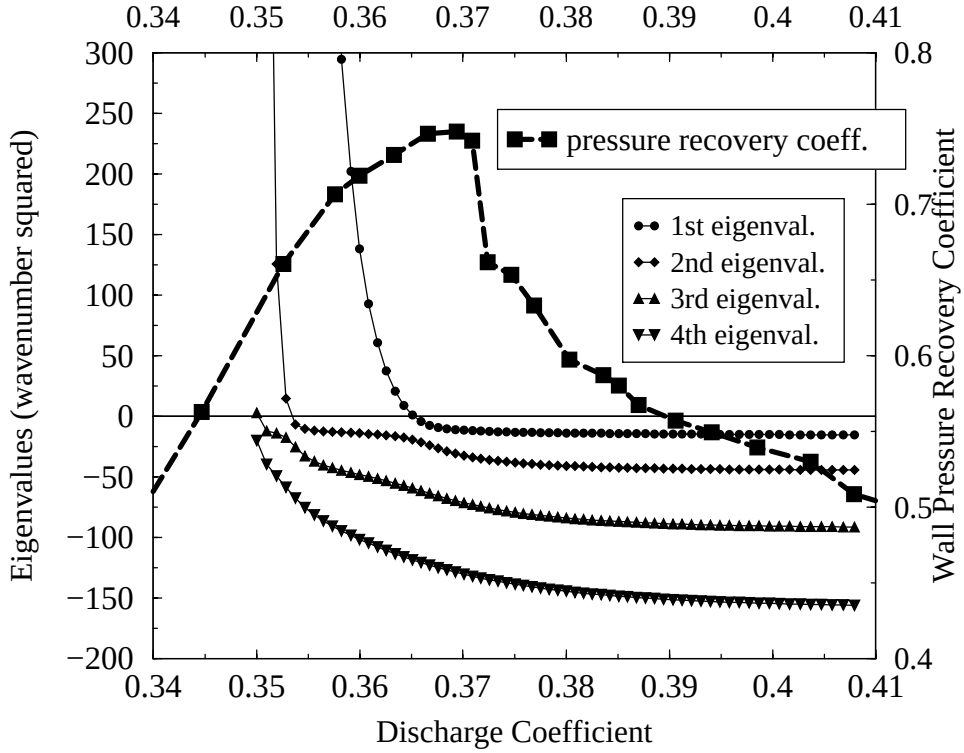

Figure 11. First four eigenvalues and the pressure recovery coefficient function of the discharge coefficient.

It is shown that the swirl reaches a critical state at discharge $\varphi = 0.365$. For larger discharge the flow ingested by the draft tube is supercritical, while at lower discharge it is subcritical. The critical state occurs quite close to the discharge $\varphi = 0.370$ where a sudden variation in the draft tube pressure recovery, as well as in the overall turbine efficiency, is experimentally observed. For the particular turbine under investigation this discharge value happens to correspond to the best efficiency point, leading to a negative impact on the turbine regulation.

Our analysis leads to the conclusion that when designing or optimizing turbine runners one should avoid reaching a critical state for the swirl at the runner outlet within the normal operating range.

ACKNOWLEDGMENTS

The authors take this opportunity to thank the partners in the FLINDT Project Eureka no. 1625: Alstom Hydro, Electricité de France, GE Hydro, VA Tech Hydro, Voith-Siemens Hydro, PSEL (Funds for Projects and Studies of the Swiss Electric Utilities), and CTI (Commission for Technology and Innovation), for their financial support.

REFERENCES

1. Avellan F. (2000) Flow Investigation in a Francis Draft Tube: the FLINDT Project, Proceedings of the 20th IAHR Symposium, Charlotte, North Carolina, U.S.A.
2. Batchelor G. K. (1964) Axial Flow in Trailing Line Vortices, Journal of Fluid Mechanics, **20**(4), pp. 645-658.
3. Benjamin T.J. (1962) Theory of Vortex Breakdown Phenomenon, Journal of Fluid Mechanics, **14**, pp. 593-629.
4. Faler J. H., and Leibovich S. (1977), Disrupted States of Vortex Flow and Vortex Breakdown, Physics of Fluids, **20**(9), pp. 1385-1400.
5. Mauri S., Kueny J.-L., and Avellan F. (2000), Numerical Prediction of the Flow in a Turbine Draft Tube. Influence of the Boundary Conditions, FEDSM'00-11084, Proceedings of the ASME 2000 Fluids Engineering Division Summer Meeting, Boston, Massachusetts, U.S.A.
6. Mauri S., Kueny J.-L., and Avellan F. (2002), Werlé-Legendre Separation in a Hydraulic Machine Draft Tube, FEDSM2002-31196, Proceedings of the ASME 2002 Fluids Engineering Division Summer Meeting, Montreal, Quebec, Canada.
7. Susan-Resiga R., Ciocan G.D., Avellan F., and Anton I. (2004) Analysis of the Swirling Flow Downstream a Francis Turbine Runner, Journal of Fluids Engineering, submitted.